Supplementary Material for

MITOCHONDRIAL SWELLING MEASUREMENT *IN SITU* BY OPTIMIZED SPATIAL FILTERING IN FLUORESCENCE MICROGRAPHS: ASTROCYTE-NEURON DIFFERENCES

Akos A. Gerencser[1,2,3], Judit Doczi[1], Beata Torocsik[1], Ella Bossy-Wetzel[3], Vera Adam-Vizi[1]

1. Department of Medical Biochemistry, Semmelweis University, Neurobiochemical Group, Hungarian Academy of Sciences, Szentagothai Knowledge Center, Budapest, Hungary;

2. Buck Institute for Age Research, Novato, CA, USA (present address)

3. Apoptosis and Cell Death Program, Burnham Institute for Medical Research, La Jolla CA, USA

FOREWORD

This document is accompanied by a Mathematica 5.2 (Wolfram Research) notebook file (ThinnessRatio.nb) which contains the original code of the simulations, simplified algorithms for the calculation of the Thinness Ratio and the optimization of the filter functions. If you don't have Mathematica on your computer, a free player can be downloaded from http://www.wolfram.com/products/player/.

3-DIMENSIONAL POINT SPREAD FUNCTION

Sub-resolution light sources are imaged as their point spread function (PSF). The PSF in the image plane is also known as an Airy disc (pattern), or an Airy body in 3 dimensions. We considered the 3D PSF of optical microscopy (from 1):

$$psf(z,r) = |I_0|^2 + 2|I_1|^2 + |I_2|^2 \qquad \text{SEq. 1}$$

$$I_0(z,r) = \int_0^\theta J_0(rk'\sin\alpha)\sqrt{\cos\alpha}\,\sin\alpha(1+\cos\alpha)e^{izk'\cos\alpha}\,d\alpha$$

$$I_1(z,r) = \int_0^\theta J_1(rk'\sin\alpha)\sqrt{\cos\alpha}\,\sin^2\alpha e^{izk'\cos\alpha}\,d\alpha$$

$$I_2(z,r) = \int_0^\theta J_2(rk'\sin\alpha)\sqrt{\cos\alpha}\,\sin\alpha(1-\cos\alpha)e^{izk'\cos\alpha}\,d\alpha$$

$$\theta = \arcsin(NA/n)$$

$$k' = 2\pi n/\lambda$$

Where *psf(z,r)* gives the intensity of the PSF as a function of radial (*r*) and axial (*z*) distance from the focal point and are given in the same units as the wavelength (λ). *n* is the refraction index of the medium, and NA is the numerical aperture. $J_x()$ is the x^{th} order Bessel function of the first kind. The 3D PSF was calculated by using Mathematica 5.2 (SFig. 1).

The confocal point spread function of an ideal laser scanning confocal microscope is calculated as follows (1):

$$psf_{conf}(z,r) = psf^2(z,r) \qquad \text{SEq. 2}$$

Or for a given pinhole:

$$psf_{conf}(z,r) = psf(z,r) \cdot (psf(z,r) \otimes pinhole(z,r)), \quad \text{SEq. 3}$$

where $\cdot$ indicates multiplication of intensities and $\otimes$ stands for convolution, and

$$pinhole(z,r) = 1 \text{ if } z=0 \text{ and } r \leq r_{pinhole} \text{ or } 0 \text{ otherwise.} \quad \text{SEq. 4}$$

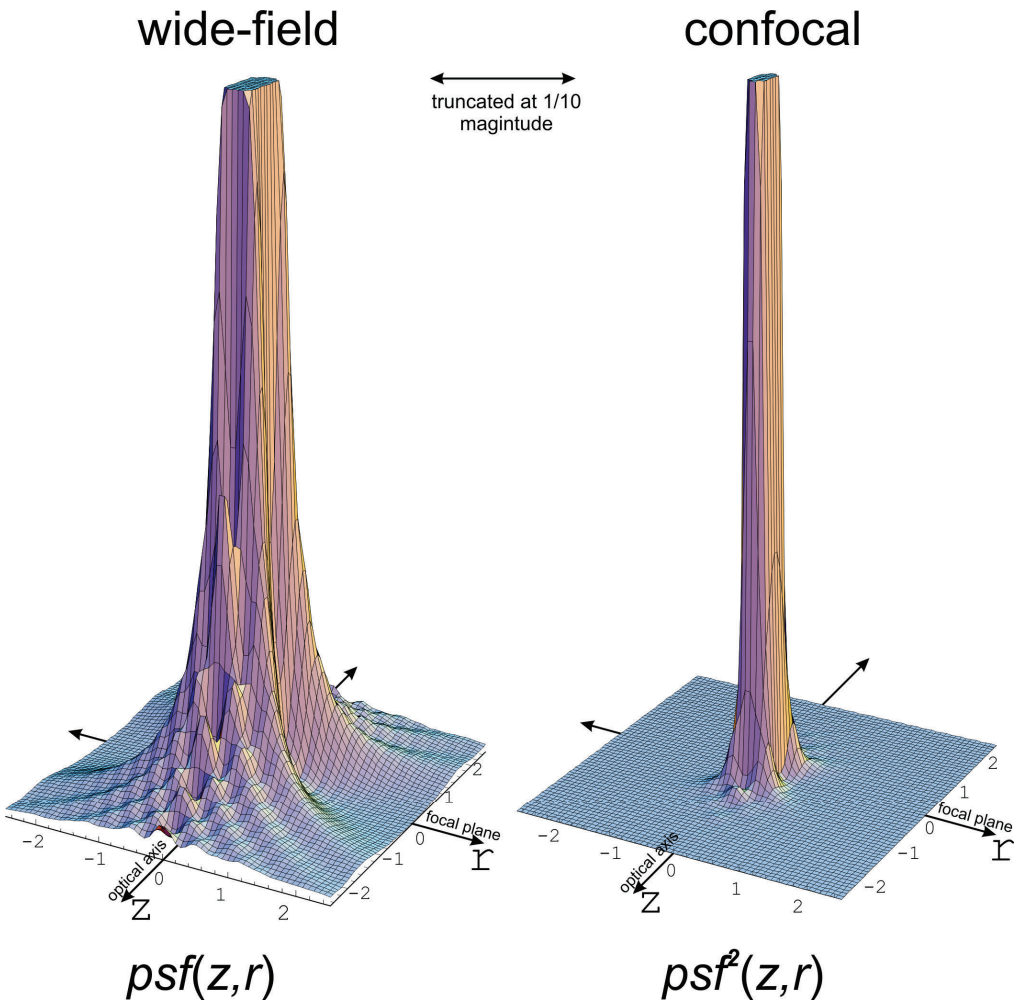

SFig. 1 Point spread functions of ideal wide-field and laser scanning confocal microscopes as calculated by SEq. 1-2. The surface shown indicates intensity as a function of radial (*r*) and axial (*z*) distance from the focal point.

THEORETICAL MODULATION TRANSFER FUNCTIONS OF OPTICAL MICROSCOPES

To assess the transmission of those spatial frequency components by the optical system which are used for Thinness Ratio (TR) calculation, the modulation transfer functions (MTFs) of wide-field and confocal microscopies were generated as the absolute

value of discrete Fourier transforms of the PSFs obtained above. The MTF gives the magnitudes of the individual spatial frequency components transmitted by the optics (http://en.wikipedia.org/wiki/Modulation_transfer_function).

The MTF can be calculated from 1D or 2D PSFs. For microscopic image formation the 2D MTF is important. The 2D PSF of an aberration free lens is a circularly symmetric function around the optical axis (SFig. 2A). The 2D MTF calculated from the 2D PSF is also circularly symmetric (SFig. 2B). We refer as MTF(ω) below as a 1D slice intersecting the origin of the 2D MTF (SFig. 2C). The MTF of a wide-field system is given by SEq. 5. The MTF of a confocal system with a given r radius of pinhole is calculated by SEq. 6 according to SEq. 3-4.

$$MTF(\omega) = MTF(\omega_x, 0) = \left| F\{psf(0,r)\} \right|, \text{ where } r = \sqrt{x^2 + y^2} \text{ for spatial domain.} \qquad \text{SEq. 5}$$

$$MTF_{conf}(\omega) = MTF_{conf}(\omega_x, 0) = \\ = \left| F\left\{psf(0,r) \cdot \mathrm{Re}\left(F^{-1}\{F\{psf(0,r)\} \cdot F\{pinhole(r)\}\}\right)\right\} \right| \qquad \text{SEq. 6}$$

In SEq.6 the · stands for multiplication of scalar or complex numbers at the corresponding spatial or frequency coordinates; ω is spatial frequency $F\{\}$ and $F^{-1}\{\}$ are 2D discrete Fourier and inverse Fourier transformations, respectively.

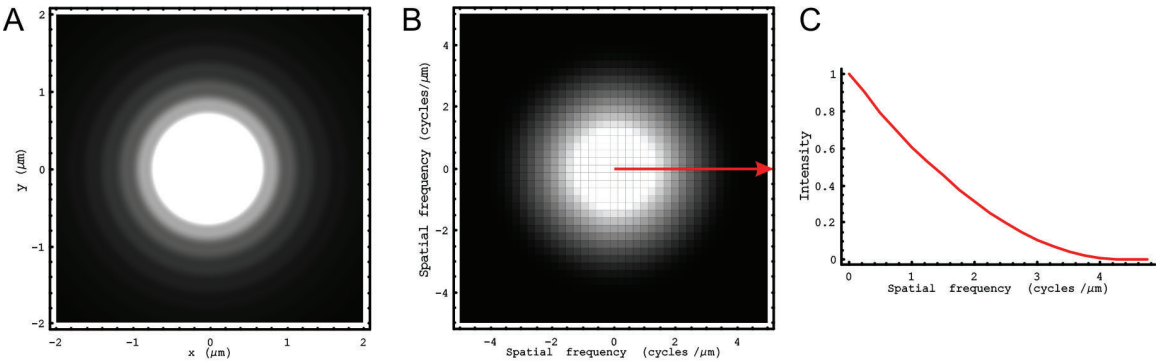

SFig. 2 Realtionship of the 2D point spread function and modulation transfer function. (A) PSF of a wide-field microscope (scaled to saturation of the middle of the diagram to show the ring pattern). (B) 2D MTF obtained by the 2D Fourier transformation of (A). (C) The MTF is a slice of the circularly symmetric MTF (B).

The MTFs of confocal systems with different pinhole diameters are shown in SFig. 3. Pinhole diameter is given here in resel (0.61λ/NA) which corresponds to the resolution of the fluorescence microscopy according to the Rayleigh's formula and is also known as Airy unit.

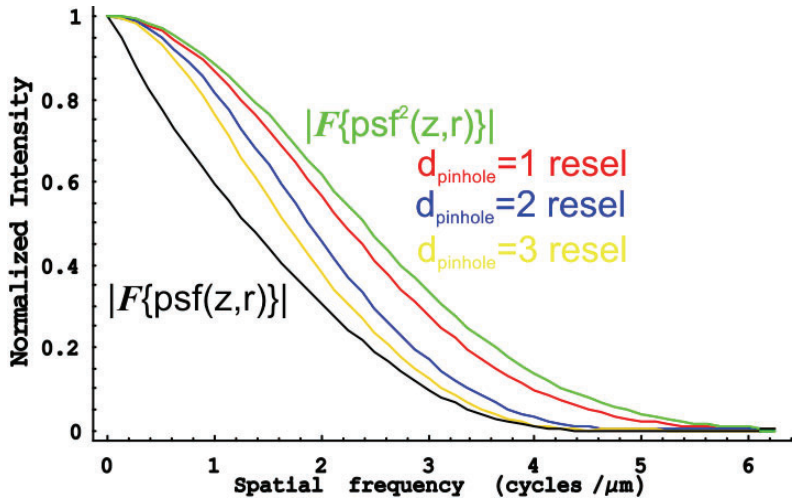

SFig. 3 Modulation transfer functions calculated as the discrete Fourier transform of the 2D point spread function in the focal plane. Traces are shown for a wide-field microscope (black), for an ideal confocal microscope (green) and for a confocal microscope with varied pinhole diameters as indicated. 1 resel= 0.61λ/NA, where λ=0.59 μm for the emission peak of DsRed2, and NA=1.3 in aqueous medium (n=1.33). (Because the excitation wavelength of DsRed2 was relatively close to the emission at λ=0.543 μm, the same psf(z,r) was used for excitation and emission during modeling of confocal microscope.)

Z-STACKING IN WIDE-FIELD AND LASER SCANNING CONFOCAL MICROSCOPY

For measurements of mitochondrial swelling in cells thicker than the depth of focus and to avoid artifacts by the drift of the focus, we used *z*-stacking and projection of the *z*-stacks into single images. This section shows that the out-of-focus blur appearing in the projected wide-field microscopic images does not deleteriously affect the TR determination.

To this end, as simplification, 1D *psf*(*z*,*r*) was calculated for *z*= -2.4; -1.6; -0.8; 0, 0.8; -1.6 and 2.4 μm focal planes (SFig. 4).

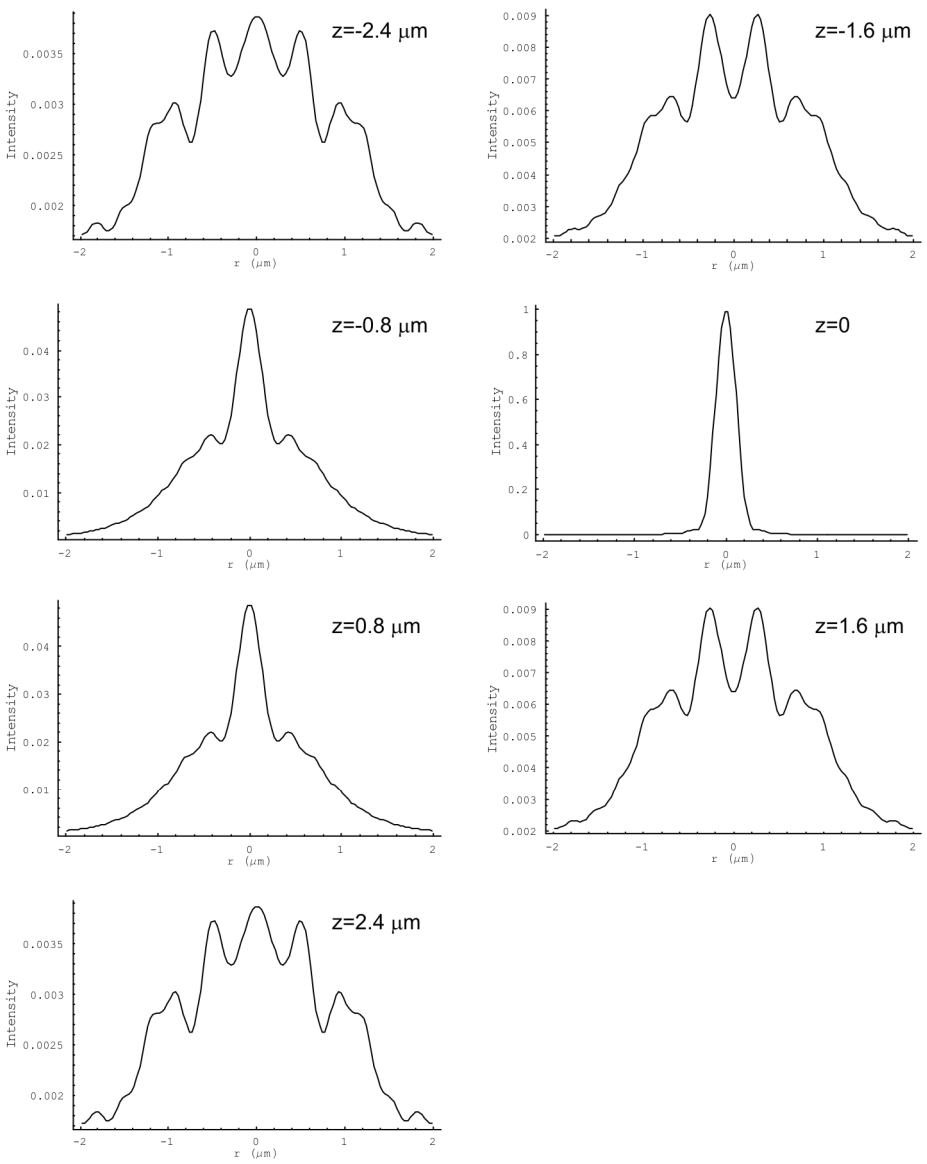

SFig. 4 1D PSFs at different distance (*z*) from the focal plane. Calculations were done for λ=0.59 μm; NA=1.3; n=1.33.

Next, considering a *z*-stack recorded over a single point source in the middle, projections of the blurred point source (thus of the out-of focus PSFs - SFig. 4) were calculated. To compare different projection methods, the maximum intensity projection and accumulation projection (summing values at each *r*) were calculated. SFig. 5 plots the in focus PSF and the projections in the top row, and the MTFs in the bottom row SFig. 5.

In wide-field microscopy the MTF of the maximum intensity projection image is similar to the in focus image, while the accumulation projection is enriched in low

frequency (haze) components. In confocal microscopy the two projections have indistinguishable effects. To maintain the range of data storage it is better to use mean intensity projection than accumulation projection.

Importantly, the high frequency components are not affected by the projection, therefore projection images are safe to use in the TR technique, with both wide-field and confocal microscopy (SFig. 5).

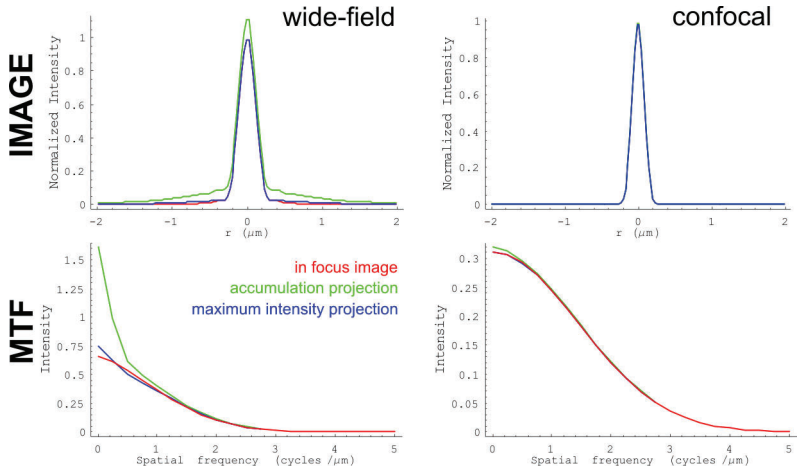

SFig. 5 Effects of *z*-projection with different methods on the PSF (top) and MTF (bottom). PSF and MTF in the focal plane are shown in red, maximum intensity *z*-projected in blue, and accumulated *z*-projected in green. Calculations were done for λ=0.59 μm; NA=1.3; n=1.33.

THE EFFECTS OF OVERLAPPING AND ADJACENT MITOCHONDRIA ON THE ACCURACY OF THE TR TECHNIQUE

The focal plane is thicker than mitochondria, especially when the focal plane is extended by *z*-stacking. Mitochondria in cells can often be found in overlapping positions or lined up following the microtubule tracks or the shape of cellular processes. Here we consider the effects of these configurations on the TR technique.

First assume elongated mitochondria crossing each other at an angle. The fluorescence of the overlapping mitochondria is additive (the overlap is brighter then the non overlapping part) within the focal plane, and also in projected *z*-stacks if mean or accumulation *z*-projection is used. The additivity is also true for the Fourier domain representation of the images, because Fourier transformation is linear (superposition of waves). Therefore the amounts of frequency components in the spectra are also additive. As a result, the TR measured over the overlapping mitochondria is equal to their arithmetic mean weighted by the intensity of the individual mitochondria. In contrast, overlapping mitochondria are detected as a single entity by binarization and segmentation based techniques, disturbing shape based roundness or thickness calculations.

Next, we considered diffraction limited microscopy of closely adjacent mitochondria. This can happen because spherical mitochondria are next to each other, or elongated mitochondria are lined up parallel. For simplicity consider a mitochondrial diameter of 1 resel (278 nm for the optical parameters used in the calculations). This is in

the range of the diameter of typical, healthy mitochondria (SFig. 6A). 1 resel diameter mitochondria touching each other are minimally resolved by optical microscopy, signified by the small notch between them in the blurred image (SFig. 6C). However, this is enough for the appearance of high frequency components smaller than the cut off frequency of the MTF (gray arrow). These frequency components can be detected by the TR technique. In contrast, these mitochondria are likely to be detected as a single entity by binarization and segmentation based techniques because the contrast between them is small. Unfortunately, if a critical amount of partial overlap occurs between aligned mitochondria (e.g. 25% of the radius in SFig. 6D) the resultant aggregate cannot be distinguished from one larger mitochondrion (SFig. 6C). However, it is not expected that many mitochondria in a cell are in this special overlap position to bias the TR when the mean of a population of mitochondria is measured.

In conclusion the TR technique is less sensitive for artifacts caused by adjacent and overlapping mitochondria, than binarization and shape measurement based techniques, which are disturbed by any extent of overlap and apposition.

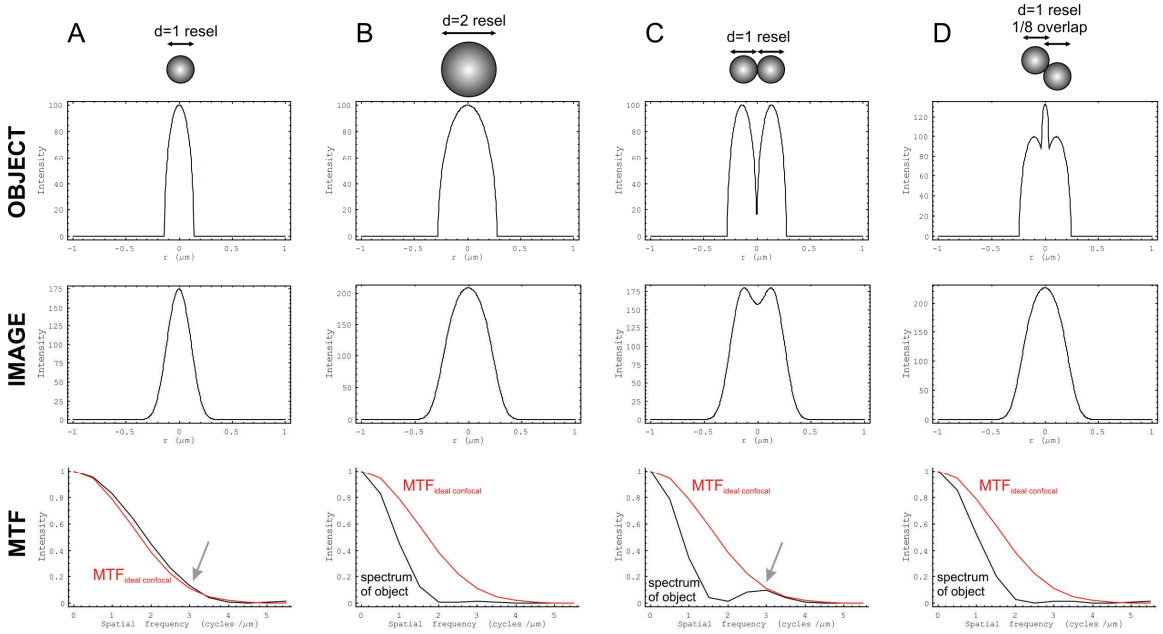

SFig. 6 Effects of near-by mitochondria on the spatial frequency components. Mitochondria were modeled in one dimension, considering the cross section of a homogeneous fluorescent sphere or rod projected into the image plane. The first row of graphs shows the intensity distribution along the focal plane of one or two mitochondria in the indicated size and spatial alignment. The second row of graphs shows mitochondria blurred by the 1D MTF of an ideal confocal microscope (SEq. 2) at λ=0.59 μm, NA=1.3, n=1.33. The bottom row shows the MTF of the microscope in red, and the spectrum of the object in black. Gray arrows indicate the presence of high frequency spectral components.

THE EFFECTS OF NUMERIC APERTURE AND PINHOLE SIZE ON SIGNAL TO NOISE RATIO OF THE TR TECHNIQUE

The detected image is the convolution of the fluorescent object and the PSF. Thinking in Fourier domain, the Fourier transform of the object is multiplied by the MTF during image formation. A small pinhole results in higher relative transmission of high spatial frequency components (SFig. 3). Because the TR is the ratio of the amplitudes of high over the low frequency components, the TR is also a function of pinhole diameter in confocal microscopy. The PSF is the richest in high frequency components as compared to larger spots that we expect to occur in the real fluorescence micrographs (we do not consider images of pure sine waves comprising only high frequency details, or pure detector/photon shot noise comprising equal amplitude low and high frequency components). Therefore the TR of the PSF gives the theoretical maximum value of the TR for the given optical configuration.

A smaller pinhole also results in decreased overall intensity, because the Airy pattern image projected on the pinhole is partially excluded, therefore photons are lost. This intensity loss is given by the convolution in SEq. 3. The smaller fluorescence intensity produces a relative increase in shot noise which deteriorates signal to noise ratio.

To decide which has a stronger effect on the signal to noise ratio (SNR) of the TR, the improved MTF or the decreased intensity by smaller pinhole diameters, we calculated the TR of the PSF and the standard deviation (SD) of the TR based on the Poisson distribution of the photon shot noise and error propagation (SEq. 7 and http://en.wikipedia.org/wiki/Error_propagation) through the ratio.

$$\sigma_f^2 = \sum_i \left(\frac{\partial f}{\partial x_i} \right)^2 \sigma_{x_i}^2 \text{, where } x_i \text{ is the } i^{\text{th}} \text{ parameter of function } f \text{ and} \qquad \text{SEq. 7}$$

$\sigma_{x_i}^2$ is the variance of the i^{th} parameter.

The MTF was obtained as the Fourier transform of the 2D confocal PSF in the focal plane for the given microscopic configuration (SEq. 6; as indicated in Article Fig. 9). The TR was calculated by the ratio of intensities given by the integrals of the MTF between 1.53-2.89 over 0.27-0.75 cycles/μm (SEq. 8). These ω_{cuton} and ω_{cutoff} pairs simulate the mixed cortical cultures – wide-field microscopy experiments (this was chosen to be uniformly used in Article Fig. 9, to show the effects of different optical configurations rather than the effects of different filter pairs).

$$I_{filter} = I_0 \int_{\omega_{cuton}}^{\omega_{cutoff}} MTF(\omega) d\omega \Big/ \int_0^{\omega_{\max}} MTF(\omega) d\omega \qquad \text{SEq. 8}$$

$$TR \pm SD = \frac{I_{high}}{I_{low}} \pm \sqrt{\frac{{I_{high}}^2}{{I_{low}}^3} + \frac{I_{high}}{{I_{low}}^2}}$$

The I_0 is the mean intensity of the PSF, I_{filter} is either I_{high} or I_{low} depending on ω_{cuton} and ω_{cutoff} frequencies of the high or the low frequency band pass filter function used for the TR technique (for simplification consider a rectangular $f_{filter}(\omega)$ instead of the Butterworth band pass and do not use normalization). The thinness ratio (TR) is given as its value±SD, considering photon shot noise ($\sigma_I^2 = I$) and the propagation of the error by SEq. 7.

By substituting *a* for the high frequency band pass filter MTF integral in SEq. 8 and *b* for the low frequency one the TR yields:

$$TR \pm SD = \frac{a}{b} \pm I_0^{-\frac{1}{2}} \sqrt{\frac{a^2 + ab}{b^3}} \qquad \text{SEq. 9}$$

Thus the SD of the TR is proportional to the -1/2 power of the mean intensity.

Finally, the signal to noise ratio (=TR/SD) was calculated for different MTFs as a function of pinhole size, NA, λ and mean intensity of the PSF (Article Fig. 9).

DIFFERENT EFFECTS OF MITOCHONDRIAL FISSION AND SWELLING ON THE THINNESS RATIO

To prepare model image sequences of mitochondria undergoing swelling and fission, zero length (*l*) mitochondria were drawn as spheres of given radius (*r*), or elongated mitochondria as *l*-long *r*-radius cylinders capped with *r*-radius half spheres at both ends (capsule bodies). The total surface (*s*) and volume (*v*) of *n* model mitochondrion are given in SEq. 10. The total surface was considered to be constant. To simulate mitochondrial fission SEq. 10 was solved for *n* and *r*, where *v* was constant (SEq. 12). For swelling the solution for *v* and *r* at a constant *n* was used (SEq. 11).

$$s = 4n\pi r^2 + 2l n\pi r$$

$$v = \frac{4}{3}\pi n r^3 + l n \pi r^2 \qquad \text{(identical to Article Eq 6)} \qquad \text{SEq. 10}$$

Solution for swelling (*n* = constant)

$$v = \frac{1}{24} l^3 n\pi + \frac{1}{12}\left(-\frac{l^2}{2} + \frac{s}{n\pi}\right)\sqrt{l^2 n^2 \pi^2 + 4n\pi s} \qquad \text{SEq. 11}$$

$$r = \frac{-l n\pi + \sqrt{l^2 n^2 \pi^2 + 4n\pi s}}{4n\pi}$$

Solution for fission (*v* = constant)

$$n = \frac{3l^2 s^2 + 144 v^2 + \sqrt{3}\,(l s - 12 v)\sqrt{3l^2 s^2 + 8 l s v + 48 v^2}}{24 l^3 \pi v} \qquad \text{SEq. 12}$$

$$r = \frac{-3 l s + 12 v + \sqrt{3}\sqrt{3l^2 s^2 + 8 l s v + 48 v^2}}{8 s}$$

The constant *v* was determined based on the initial *n* and *l* and on *s*/*v* (sperv) to simulate fission starting with the same number of mitochondria, but with different *s*/*v* values.

$$v_{const} = \frac{3n\pi(48 + l^2 \text{sperv}^2) - \sqrt{3}\,\pi\sqrt{n^2(-12 + l\,\text{sperv})^2(48 + l\,\text{sperv}(8 + 3l\,\text{sperv}))}}{8\,\text{sperv}^3}$$

Images of mitochondrion models (at 512x512 pixel) were generated by setting the length and radius of solid and fluorescent capsule bodies according to the calculated parameters. The projected (integrated) intensity in the image plane was calculated by SEq. 13.

$$f(z)=\frac{100}{r}\sqrt{r^2-z^2} \text{ if } z^2<r^2 \text{ or 0 otherwise,} \qquad \text{SEq. 13}$$

where z is the distance from the centerline or center of the capsule body or sphere, respectively. To achieve sub-pixel accuracy, bilinear interpolation (http://en.wikipedia.org/wiki/Bilinear_interpolation) was used (SEq. 14; SFig. 7A).

$$g(x,y)=\begin{bmatrix}0.5 & 0.5\end{bmatrix}\begin{bmatrix}h(x+0,y+0) & h(x+0,y+1)\\ h(x+1,y+0) & h(x+1,y+1)\end{bmatrix}\begin{bmatrix}0.5\\0.5\end{bmatrix}= \qquad \text{SEq. 14}$$

$$=0.25\left(h(x+0,y+0)+h(x+0,y+1)+h(x+1,y+0)+h(x+1,y+1)\right)$$

$$h(x,y)=f\left(\sqrt{(x-x_0-0.5)^2+(y-y_0-0.5)^2}\right), \qquad \text{SEq. 15}$$

In SEq. 14-15 $g(x,y)$ is a pixel of the image at (x,y) position, and $h(x,y)$ yields the fluorescence intensity of the r-radius spherical model mitochondrion centered at (x_0,y_0). In practice the bilinear interpolation simplifies to the arithmetic mean of the intensities in the corner points of the pixel, because it was calculated for the midpoint of the pixel (SEq. 14). Capsule bodies were calculated in a similar way, but the distance was measured form the center line instead of SEq. 15. This calculation resulted “anti aliased” pictures of spheres and capsule bodies with pixel intensities reflecting the extent of overlap between the pixel and the edge of the calculated model (SFig. 7A). While this method of drawing spheres and capsule bodies proved to be accurate at diameters above 2 pixels, below this size moiré patterns appeared resulting in higher TR values than expected. Therefore model images were composed at 2048x2048 pixel resolution by drawing four times larger models, followed by demagnification to the 512x512 size by taking the average of every 4x4 pixel, like binning in CCD cameras.

Importantly, all model images had the final resolution of 512x512 pixel. The images were calibrated to 0.1 μm/pixel or 0.075 μm/pixel to align to the wide-field and confocal microscopic experiments, respectively. Therefore the interpolation was affecting only the way of drawing model mitochondria in the images, but not the dimensions or the scaling of the images.

The n number of mitochondria were placed in random positions and orientations, either identically or changing from frame to frame on the model images (SFig. 7). In the case of overlaps the intensity was additive. Of note, extreme increases in the amounts of models slightly affected the TR-calculation, with a small increase of the TR when the amounts of models were increased (the number of pixels occupied, rather than the number of models). Importantly, this did not affect or bias our conclusions, and such extreme changes were never seen in biological experiments.

To simulate the blur of the microscope lens, model images were convolved with the theoretical 2D PSF for the given image acquisition condition. For convolution the same algorithm was used as for the band pass filtering, but the corresponding MTFs (given in SFig. 3) were used as filter function. Importantly, the MTF was always calculated for the

same μm/pixel scaling that the model image intended to have. Of note, there was no difference between TR values obtained in blurred images generated as described above or when the 2048x2048 pixel images were blurred with a scaled MTF followed by demagnification, when the diameters were above 2 pixels. To avoid moiré patterns in images for Article Fig 3C-D blurring was done on the 2048x2048 pixel images, while more conveniently (CPU and memory-wise), the demagnified images were blurred for the rest of the simulations. After blurring, intensities were scaled for each frame to span between 0 and 1000.

The resultant blurred model images were processed to obtain TR in the same way as images acquired by microscopy.

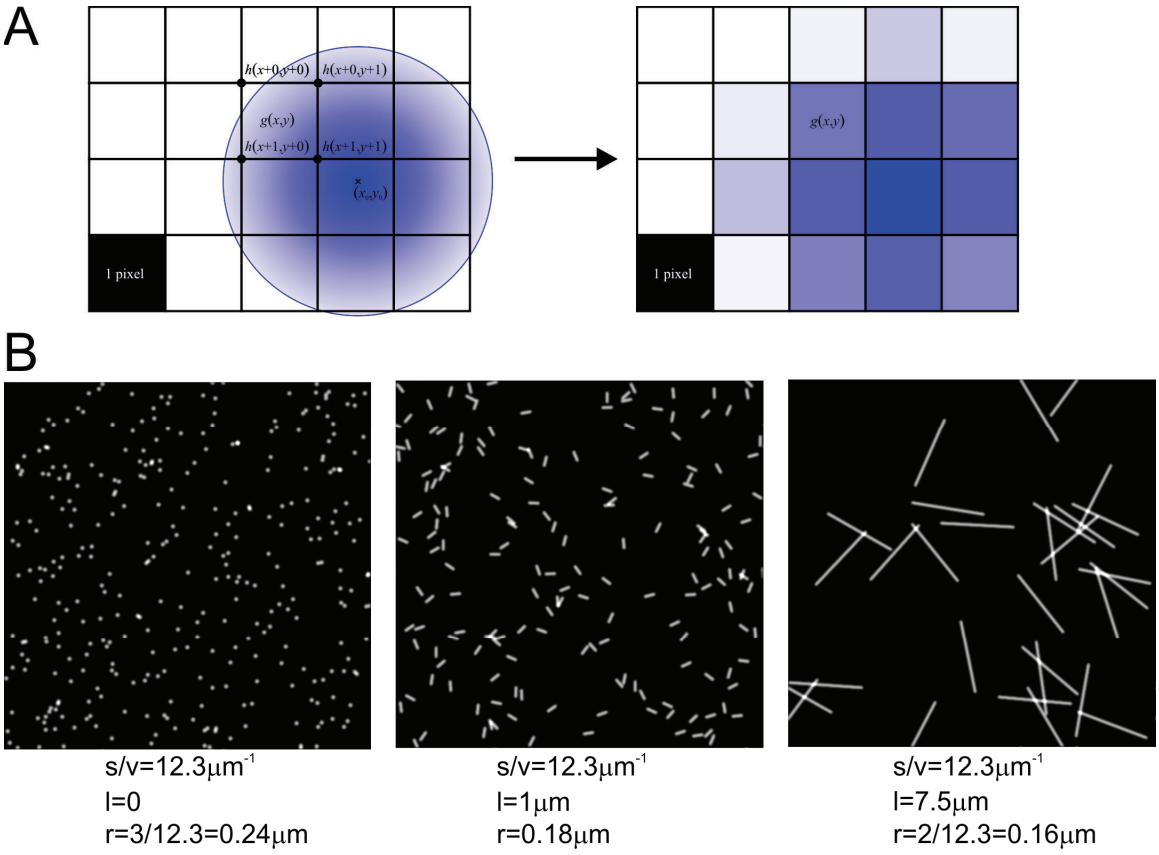

SFig. 7 Model mitochondrion images. A: Scheme of bilinear interpolation corresponding to SEq.14-15. B: Representative model images calculated for the confocal microscopic configuration (0.075 μm/pixel resolution and blurring corresponding to λ=0.59 μm, NA=1.3, n=1.33 and 1.2 resel pinhole).

The following data supports Article Figure 4 by showing the simulation results for all the three optical configurations used.

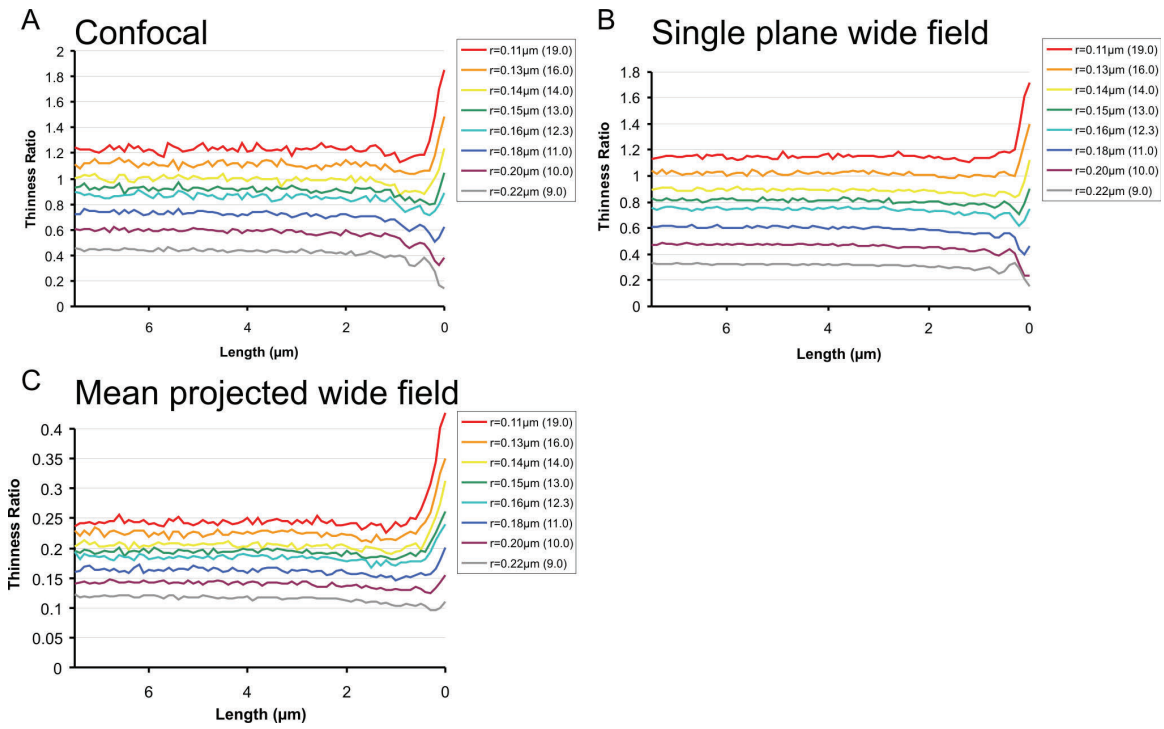

SFig. 8 Effects of mitochondrial fission with the indicated starting r (or constant s/v) on the TR. Model mitochondria were generated, blurred and the TR was calculated according to the experimental conditions or parameters in the Article: A: astrocytes with wide-field microscopy; B: neurons with confocal microscopy; C: mixed cultures with projected wide-field microscopy. See the corresponding MTFs used for blurring and filter functions used for the TR calculation in Article Fig. 2B-D.

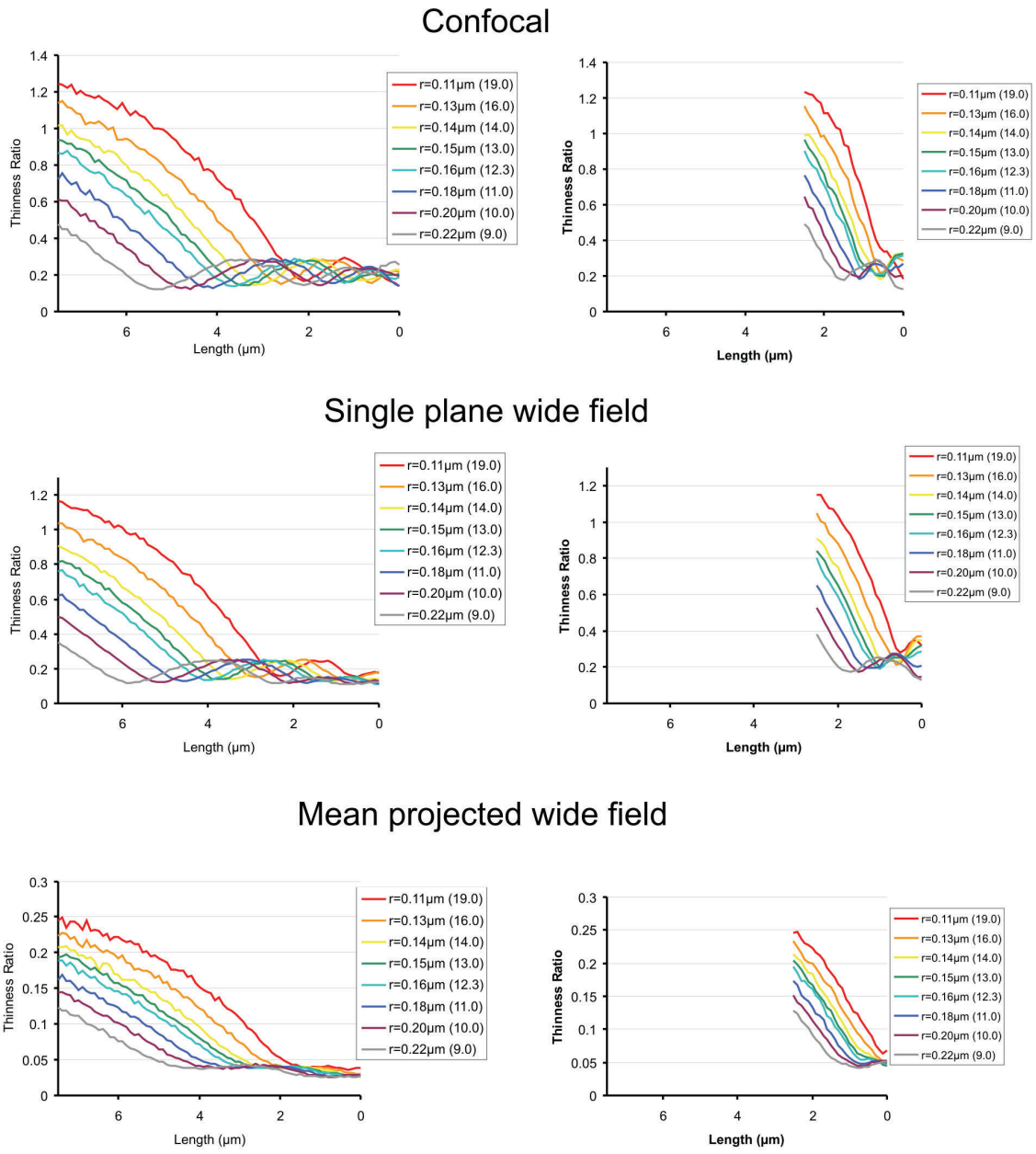

SFig. 9 Effects of mitochondrial swelling with different starting r (or s/v) on the TR calculated in different image acquisition configurations. See the corresponding MTFs used for blurring and filter functions used for the TR calculation in Article Fig. 2B-D.

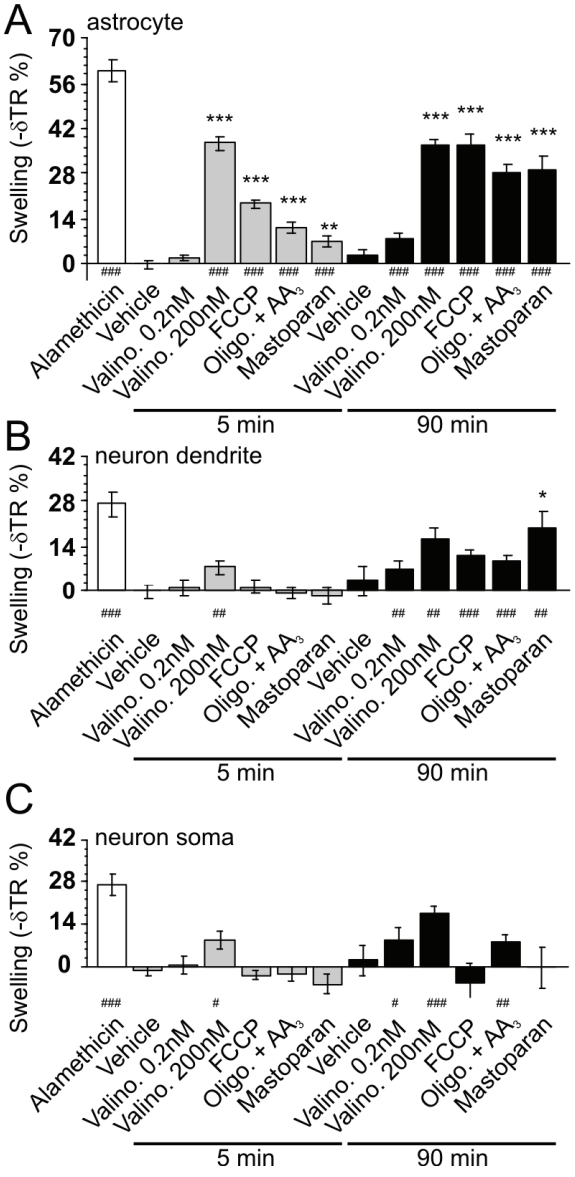

SFig. 10 Comparison of astrocytes and neurons in mixed cortical cultures using TR technique filter functions optimized in alamethicin-treated neurons. Corresponds to Article Fig. 10. (A-C) Mitochondrial swelling is indicated in percentage of negative change of the TR. The TR filter functions were optimized on the effect of alamethicin in a set of three neurons. The TR was measured at baseline, after 5 and 90 min treatment with vehicle (1:1000 ethanol), valinomycin (0.2 and 200 nM), FCCP (1 μM), oligomycin (2 μg/ml) plus antimycin A_3 (1 μM) or mastoparan (10 μM). Bars indicated mean±s.e.m. of baseline normalized negative TR for the 5 min treatment (gray bars) or the 90 min treatment (black bars). The maximal effect alamethicin (20 μg/ml) was captured after addition without time lag, because of progressive lysis of mitochondria. #, ## and ### significance at p<0.05, 0.01 and 0.001, respectively compared to 0 by two sided Student *t*-test. *, ** and * significance at p<0.05, 0.01 and 0.001, respectively compared to the vehicle treatment by ANOVA for the given time point with Dunnett post-hoc test.**

Reference List

1. Webb, R. 1996. Confocal optical microscopy. Rep. Prog. Phys. 59:427-471

2. Yuste, R., F. Lanni, and A. Konnerth. 2000. Imaging Neurons. Cold Spring Harbor Laboratory Press.